Journal of Science and Technology ─ Smart Systems and Devices
Volume x, Issue x, Month Year, ppp–ppp

TRV Assessment of 500-kV Shunt Reactor Switching Using Black-Box Circuit-Breaker Arc Models in ATPDraw

Trung-Son Nguyen*, Hung Chu Huu Tuan, Hung Dang Duc
Hanoi University of Science and Technology, Ha Noi, Vietnam
**Corresponding author email: son.nguyentrung@hust.edu.vn*

Abstract

Frequent switching of 500-kV shunt reactors for voltage and reactive-power regulation can produce severe transient recovery voltage (TRV), current chopping, and reignition across circuit-breaker contacts. This paper proposes a practical standard-based dielectric recovery algorithm for high-voltage SF6 circuit breakers and couples it with three dynamic arc equations, namely the Cassie-Mayr, Schwarz-Avdonin, and Schavemaker models. The proposed algorithm replaces unavailable manufacturer-specific dielectric recovery curves with a dielectric-recovery screening reference derived from circuit-breaker catalogue information and IEC TRV requirements, thereby allowing reignition and restrike decisions to be included in ATPDraw simulations. The models are implemented in MODELS as black-box circuit-breaker representations and are compared with the built-in ATP breaker model for a 128-Mvar shunt reactor in a Vietnamese 500-kV transmission system. The Phase-A peak TRV increases from 870 kV with the default ATP breaker to 874 kV, 946 kV, and 1600 kV with the Cassie-Mayr, Schwarz-Avdonin, and Schavemaker models, respectively. The mitigation study shows that a surge arrester reduces the Cassie-Mayr reference TRV to 840 kV, while the combined surge-arrester and neutral-grounding-disconnector configuration further reduces it to 774 kV. The adopted network, arc-model, TRV-envelope, and reignition parameters are reported to support reproducibility. The obtained values should be interpreted as comparative engineering estimates rather than manufacturer-specific breaker ratings.

Keywords: ATPDraw, breaker-duty assessment, circuit-breaker arc model, mitigation measures, shunt-reactor switching, standard-based dielectric recovery algorithm, transient recovery voltage.

In press

1. Introduction

Shunt reactors are widely used in extra-high-voltage transmission systems to control voltage and reactive power during light-load operation and are subjected to numerous switching operations over their service life [1-2]. IEEE Std C37.015 identifies shunt-reactor switching as a special application duty because the interrupted current is small, highly inductive, and sensitive to the recovery voltage imposed on the circuit breaker [1]. Reactors are typically disconnected during peak-load periods and reconnected under light-load conditions; they may also be switched for scheduled maintenance or for corrective actions following network disturbances.

Both energization and de-energization of a shunt reactor can produce overvoltages, inrush or trapped-charge phenomena, and recovery-voltage stresses that may influence insulation coordination and protection settings [3-4]. During de-energization, interruption of the small inductive current creates a risk of current chopping and circuit-breaker reignition. Reignition occurs when the TRV across the opening contacts exceeds the recovering dielectric withstand of the contact gap [5]. If this process is not represented in simulation, the calculated switching duty may be optimistic.

The de-energization of shunt reactors using SF6 circuit breakers has been studied extensively, and reignition-related interrupter damage leading to breaker failure is well documented [4, 6]. This issue has become more critical as SF6 breaker designs have evolved, for example through the reduction in the number of series breaks and the removal of grading capacitors [6]. Nevertheless, properly specified and type-tested circuit breakers, combined with point-on-wave opening control to minimize the likelihood of reignition, remain a proven solution for preventing interrupter damage [1, 6].

In 500-kV substations, switching of line and busbar shunt reactors is a routine but severe duty for the circuit breaker because the interrupted current is small, highly inductive, and sensitive to dielectric recovery [1, 3, 4]. Under these conditions, transient recovery voltage (TRV), current chopping, high-frequency oscillation, and reignition may occur after contact separation. If these phenomena are not properly represented in simulation, the resulting dielectric stress may be underestimated.

Numerous dynamic arc models for circuit breakers have been developed, particularly for gas-type interrupters such as air-blast and SF6 circuit breakers [7-9]. These models are effective for representing the thermal arc phase because they calculate the

p-ISSN 3093-3285
e-ISSN 3093-3315
https://doi.org/10.51316/jst.xxx.ssad.2026.36.x.x
Received: Apr 25, 2026; Revised: May 26, 2026;
Accepted: Jun 21, 2026; Online:Jul 8, 2026

time-varying arc conductance from the instantaneous voltage-current history. However, the arc equations alone do not describe the dielectric recovery of the contact gap; therefore, reignition and restrike phenomena cannot be determined directly from the arc equations. In [5], an algorithm was introduced to incorporate dielectric recovery into the ignition and reignition process of vacuum circuit breakers. In the present high-voltage application, the investigated circuit breakers are SF6 types, but manufacturer-specific dielectric recovery curves are not available. In practice, manufacturers usually provide catalogue data and compliance information based on circuit-breaker standards rather than detailed dielectric recovery curves.

To address this limitation, this paper proposes a practical standard-based dielectric recovery algorithm inspired by the logic in [5], but adapted for high-voltage SF6 circuit breakers whose dielectric recovery curves are unavailable. The proposed algorithm constructs a dielectric-recovery screening reference from circuit-breaker catalogue data and IEC four-parameter TRV requirements, and then couples this reference with well-known dynamic arc equations from the literature, namely the Cassie-Mayr, Schwarz-Avdonin, and Schavemaker models. The main contribution is therefore not a new arc equation, but a practical coupling method that enables arc-equation-based breaker modelling and standard-based dielectric recovery assessment to operate together in ATPDraw/MODELS.

On this basis, the paper develops an integrated ATPDraw/MODELS implementation, reports a transparent parameter set, compares three established black-box arc models under the same 500-kV shunt-reactor switching condition, and evaluates two practical mitigation measures. The study examines circuit-breaker TRV at a practical engineering level, where the main objective is breaker-duty screening and mitigation comparison rather than manufacturer-specific interrupter design. The remainder of the paper is organized as follows:

- Section 2 reviews the related work, standards basis, and fundamental breaker-switching theory.
- Section 3 presents the ATP/EMTP model development and the proposed standard-based dielectric recovery algorithm.
- Section 4 provides the TRV analysis results and different mitigation strategies.
- Section 5 summarizes the conclusions with respect to the study objectives.

2. Related Work and Circuit-Breaker TRV Theory

2.1. Related Works and Standards Basis

Previous work on shunt-reactor switching provides three foundations for this study. First, EMTP investigations of shunt-reactor switching have shown that source impedance, reactor stray capacitance, trapped charge, and breaker representation strongly influence the calculated recovery voltage [3-4]. Second, studies of voltage escalation and reignition have established that high-frequency current interruption after reignition can produce repeated overvoltage pulses and non-uniform winding stress [10-12]. Third, black-box circuit-breaker models such as Cassie-Mayr, Schwarz-Avdonin, and Schavemaker are widely used when the external voltage-current behaviour of the interrupter is more important than the internal gas-flow physics [7-8].

The standards basis is taken from IEEE Std C37.015 for shunt-reactor switching applications and IEC 62271-100 for TRV envelope definitions [1, 13]. In this paper, the IEC four-parameter envelope is used as a practical dielectric-recovery screening reference, while IEEE Std C37.015 is used to frame the switching duty, mitigation options, and interpretation of results. This combination is appropriate for comparative EMTP studies, but it does not replace a circuit-breaker type test or a manufacturer-specific dielectric recovery curve.

2.2. Current Chopping

When interrupting an inductive current, current chopping may occur before the natural current zero [14-15]. The arc and the surrounding capacitances can create a high-frequency oscillatory component that forces the instantaneous current to zero. If the breaker interrupts at this artificial zero, the magnetic energy stored in the reactor is transferred to the equivalent capacitance on the load side, producing an overvoltage governed by the energy balance in (1) [14, 16].

$$\frac{1}{2}CV^2 = \frac{1}{2}Li^2 + \frac{1}{2}CV_0^2 \tag{1}$$

which shows that the final electric energy stored in the capacitor equals the sum of the initial magnetic energy in the inductor and the initial electric energy in the capacitor [14, 16]. In this relationship, the maximum overvoltage depends on the chopping current and the voltage immediately before interruption, which is approximately equal to the supply voltage.

Typical chopping-current values for existing circuit breakers are in the range of several amperes to several tens of amperes [14]. For a fixed chopping current, the overvoltage increases with reactor inductance; therefore, lower-rated or lightly loaded reactors may experience relatively high switching overvoltages. The capacitance still remains important because it controls the natural oscillation frequency and the RRRV seen by the breaker.

2.3. Reignition Phenomenon

After current interruption, the voltage across the circuit-breaker contacts rises gradually. If the contact gap is too small, electrical breakdown may occur and a new arc is initiated between the breaker contacts. This phenomenon is known as reignition because the dielectric strength of the contact gap does not recover

In press

fast enough to withstand the imposed TRV [5, 12]. In practice, dielectric recovery is not fully deterministic; it is influenced by gas temperature, pressure, contact condition, and breaker operating dispersion. For this reason, both deterministic and probabilistic breaker models are relevant in reactor-switching studies.

The dielectric strength is normally not provided directly by manufacturers; however, IEC 62271-100 [13] defines two-parameter and four-parameter TRV test envelopes that can be used as practical engineering references. In the present study, these IEC curves are used as screening envelopes for reignition assessment rather than as breaker-specific dielectric recovery characteristics.

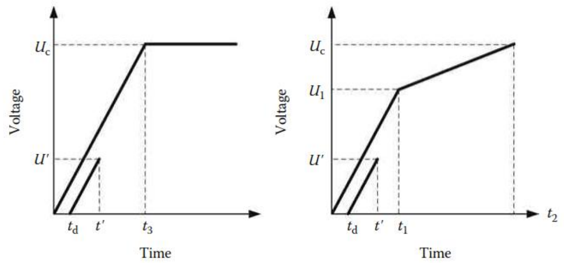

Fig. 1. IEC two- and four-parameter limiting curves

Both the TRV magnitude and its initial slope, known as the rate of rise of recovery voltage (RRRV), should remain below the adopted envelope with an appropriate safety margin. If the calculated TRV exceeds this reference envelope, reignition may occur. The adopted TRV envelope is therefore used here as an engineering screening criterion for reignition susceptibility in comparative studies, rather than as a direct physical dielectric recovery model.

During reignition, charges stored in nearby capacitances oscillate rapidly through small inductances on both sides of the breaker. This process produces very high-frequency overvoltages, often reaching several hundred kilohertz, at the reactor terminals [10-12]. Such high-frequency overvoltages tend to concentrate on the coil turns closest to the terminals in devices such as reactors, transformers, and motors. Although the magnitude of the reignition overvoltage may be lower than that caused by current chopping, its high frequency creates severe electrical stress that surge arresters cannot always mitigate effectively. To prevent insulation failure and ensure system reliability, especially in high-voltage systems such as 300-kV and 550-kV networks, measures such as improving insulation strength, enhancing circuit-breaker performance, and controlling contact-separation timing are applied.

2.4. Multiple Reignition

The current caused by reignition can reach several kiloamperes and very high frequencies [10-11]. Because of the rapid rate of current change near zero, circuit breakers often cannot interrupt it immediately. However, the current decays quickly and can eventually be interrupted at lower amplitudes. During this process, electromagnetic energy stored in the coil can generate overvoltages similar to or even greater than those caused by current chopping, depending on conditions.

In some cases, reignition may occur repeatedly; this phenomenon is called multiple reignition [10, 12]. Although rare, it can produce extremely severe overvoltages. The likelihood of multiple reignitions depends on system conditions, which are typically fixed. Since multiple reignitions lead to uncontrollable and dangerous overvoltages, the most effective prevention strategy is to avoid the initial reignition altogether.

2.5. Circuit-breaker Interruption Procedure

When reignition takes place, the load-side voltage is rapidly pulled toward the source-side voltage, producing steep-front overvoltage pulses [5, 11]. These pulses may result in non-uniform voltage distribution in the reactor winding and impose repeated stress on both the reactor insulation and breaker contacts. The breaker must then attempt to interrupt the resulting high-frequency current at subsequent zero crossings.

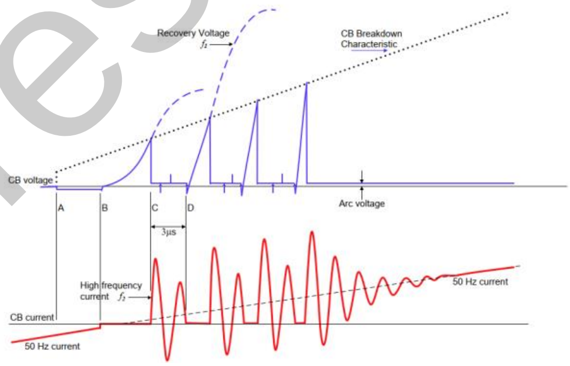

Fig. 2. Ignition and reignition oscillogram for an unsuccessful interruption

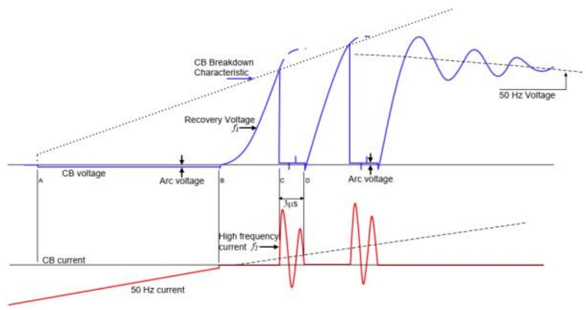

Fig. 3. Ignition and reignition oscillogram for a successful interruption

According to Fig. 2, in an unsuccessful interruption the TRV exceeds the dielectric strength at point C, which triggers reignition and generates a high-frequency current. Point D denotes the next high-frequency current zero after reignition in both Fig. 2 and Fig. 3. The difference between the two figures is the breaker condition at point D: in Fig. 2 the thermal and dielectric

In press

recovery conditions are not satisfied and the arc continues into the next power-frequency cycle, whereas in Fig. 3 the high-frequency current is successfully extinguished at point D and the breaker returns to the open state. This distinction clarifies that point D is a comparable current-zero instant, but the interruption outcome is different in the two figures.

2.6. Circuit-breaker Model

The primary goals of a circuit-breaker model are twofold: from a system perspective, to calculate all voltages and currents that arise in the network because of breaker operation; and from a breaker perspective, to assess whether the breaker can successfully interrupt current under specific system conditions [7-8].

A black-box model focuses on describing how the circuit breaker interacts with the electrical system during the interruption process [7-8]. Instead of analyzing internal physical processes, it emphasizes the external electrical behavior of the breaker. The objective is to achieve an accurate quantitative representation of breaker performance.

Different levels of model complexity can be used:

1. Ideal switch model (Simplest)

This model assumes perfect interruption independent of the arc [7, 14]. The breaker is represented as an ideal switch that opens at the first current zero after a trip signal. It can be used to determine the voltage across the breaker and compare it with its transient recovery voltage (TRV) capability. However, it does not account for any interaction between the arc and the system.

2. Predefined arc model

A more detailed model represents the arc as a time-varying resistance or conductance [7-8]. Its variation is predetermined based on breaker characteristics and initial current conditions. This model can simulate the influence of the arc on the system but requires prior knowledge of arc behavior, which is often difficult to obtain. It also still depends on precomputed TRV curves for evaluation.

3. Dynamic arc model (Most advanced)

The most sophisticated approach models the breaker as a resistance or conductance that changes dynamically based on the history of arc voltage and current [7-8]. This allows simulation of both the effect of the arc on the system and the effect of the system on the arc. This model eliminates the need for predefined TRV curves. It is mainly used to analyze arc extinction during the thermal phase, although some versions can also study reignition caused by insufficient dielectric strength. Common applications include short-line fault interruption and switching of small inductive currents.

Dynamic arc models are widely implemented in electromagnetic transient programs (EMTP) and are effective for simulating the thermal phase of current interruption [7-9]. Some models can also represent both the thermal and dielectric phases, particularly for SF6 circuit breakers. In the present study, the circuit breakers are represented using dynamic arc models with different governing equations, coupled with an algorithm that accounts for circuit-breaker insulation recovery.

3. System Modelling in ATP-EMTP

Shunt reactor switching is an operation in which small differences in circuit parameters can produce large differences in duty severity [1, 3, and 4]. This section presents the development of the study test model.

3.1. System Description

The investigated switching circuit consists of a 520-kV source, a three-phase circuit breaker, and a 128-Mvar shunt reactor, as illustrated in Fig. 4. The purpose of the model is to analyze electromagnetic transients during no-load shunt-reactor switching and to evaluate the effect of breaker arc representation on the resulting TRV.

The model is divided into three main blocks: the source block, the circuit-breaker block, and the shunt-reactor block.

- Source block: source voltage together with the equivalent source resistance and inductance.
- Circuit breaker block: three-phase breaker (SW1) represented either by the built-in ATP breaker (3-phase time-controlled switch) or by MODELS-based arc formulations.

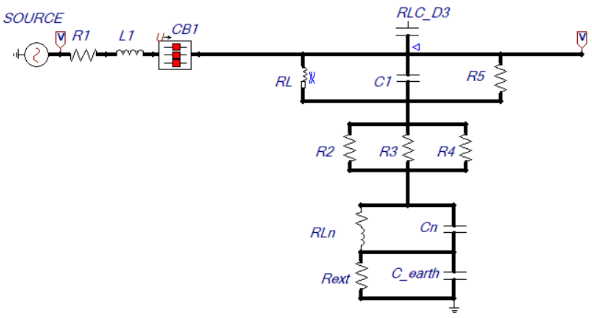

Fig. 4. ATP simulation diagram of 500-kV shunt reactor switching

- Shunt reactor block: reactor branch, parasitic capacitances, leakage resistances, neutral reactor, grounding resistance, and grounding capacitance required to reproduce the transient oscillatory behavior after switching.

The values of the main elements are listed in Table 1. The table includes the source parameters, shunt-reactor data, parasitic capacitances, neutral branch, and grounding quantities used to represent the dominant TRV oscillation paths, following the data reported in [6, 18].

in press

Journal of Science and Technology — Smart Systems and Devices
Volume x, Issue x, Month Year, ppp–ppp

The 128-Mvar shunt reactor is represented by its phase resistance and inductance together with the terminal-to-ground and neutral-point parasitic capacitances that determine the high-frequency TRV oscillation. The inductance value is consistent with $L = V_{LL}^2/(\omega Q)$ for a 500-kV, 128-Mvar reactor at 50 Hz, giving approximately 6.2 H per phase. The source resistance and inductance are the Thevenin equivalent of the upstream 500-kV network in the study case [6]. Because shunt-reactor TRV is sensitive to small capacitances and neutral-side conditions, the stray capacitances and neutral/grounding elements are listed explicitly rather than being hidden in the ATPDraw schematic [6, 18].

Table 1. Key simulation parameters

Parameter	Symbol	Value	Unit
System voltage (line to line rms)	SOURCE	520	kV
Source resistance	R1	0.8	Ω
Source inductance	L1	22.9	mH
Delta-connected capacitance	RLC_D3	0.00075	µF
Auxiliary series resistance	RL	3.904	Ω
Auxiliary series inductance	RL	4973.5	mH
Shunt-reactor phase resistance	RL	4.88	Ω
Shunt-reactor phase inductance	RL	6217	mH
Parasitic capacitance	C1	0.00128	µF
Leakage resistance	R5	200000	Ω
Parallel resistance	R2, R3, R4	0.01	Ω
Neutral-reactor resistance	RLn	5	Ω
Neutral-reactor inductance	RLn	2069.01	mH
Grounding resistance	Rext	40	Ω
Neutral-point parasitic capacitance	Cn	0.0061635	µF
Grounding capacitance	C_{earth}	1.57E-5	µF

3.2 Circuit Breaker Model

The built-in ATP breaker component is suitable for general switching studies; however, detailed investigation of current chopping, arc extinction, and reignition requires an explicit dynamic arc model. Therefore, this study implements the Cassie-Mayr, Schavemaker, and Schwarz-Avdonin formulations in the MODELS environment to reproduce the time-varying conductance of the breaker arc during current interruption [7-8].

The arc behaviour is implemented in ATPDraw through a Type-91 TACS/MODELS block coupled to the electrical network [8, 16]. At every time step, the model receives the instantaneous breaker current and contact voltage, solves the selected conductance differential equation, and returns the equivalent arc resistance to the network solution. This closed-loop representation is needed because the network transient affects the arc conductance, while the arc conductance simultaneously changes the calculated TRV.

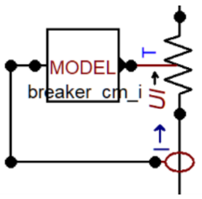

Fig. 5. Breaker arc model using Type91 TACS block in ATPdraw

3.2.1. Cassie-mayr model

The Cassie model is appropriate for the high-current region, whereas the Mayr model better represents arc behavior near current zero. In practical interruption studies, neither model alone is sufficient over the full current range. A composite Cassie-Mayr model is therefore adopted so that the breaker arc can be described continuously from the high-current regime to the extinction region [4], [8].

$$\frac{1}{g_c} \times \frac{dg_c}{dt} = \frac{1}{\tau_c}\left(\frac{i^2}{U_{arc} g_c} - 1\right) \tag{2}$$

$$\frac{1}{g_m} \times \frac{dg_m}{dt} = \frac{1}{\tau_m}\left(\frac{i^2}{P_0 g_m} - 1\right) \tag{3}$$

$$\frac{1}{g} = \frac{1}{g_m} + \frac{1}{g_c} \tag{4}$$

In these equations, g is the arc conductance, U_{arc} is the constant part of arc voltage, i is the arc current, and τ_c and τ_m are the Cassie and Mayr arc time constants, respectively. P_0 is the steady-state power loss, g_c is the arc conductance in the Cassie portion, and g_m is the arc conductance in the Mayr portion. The overall arc conductance g is obtained from the parallel conductance relation in (4).

3.2.2. Schwarz-avdonin model

The Schwarz-Avdonin arc model is an extension of the Mayr model that takes into account the dependence of the arc time constant and the dissipated power on arc conductance, as expressed below [8]:

$$\tau = \tau_0 g^a \tag{5}$$

$$P_{loss} = P_0 g^b \tag{6}$$

In press

Each of these four parameters characterizes the arc as a nonlinear resistance and describes the variation of conductance with time, as shown below.

$$\frac{1}{g}\times\frac{dg}{dt}=\frac{1}{\tau}\left(\left(\frac{P_{\text{supp}}}{P_{\text{loss}}}\right)-1\right) \qquad (7)$$

where a and b are fitting coefficients, g is the arc conductance, τ_0 is the initial arc time constant, τ is the conductance-dependent arc time constant, P_0 is the initial breaker cooling power, P_{supp} is the instantaneous electrical power supplied to the arc (P_{supp} = ui), and P_{loss} is the cooling or loss power. The parameters *a* and *b* control how the time constant and cooling power change as the arc conductance decreases.

3.2.3. Schavemaker model

The Schavemaker arc model is a modified version of the Mayr arc model. It uses a constant time parameter based on current-zero measurements and a cooling power expressed as a function of the electrical power input [8]. This model consists of a single differential equation that is applicable in both the high-current and low-current regions, as shown below:

$$\frac{d\ln g}{dt}=\frac{1}{\tau}\left(\frac{P_{\text{supp}}}{\max(U_{\text{arc}}\mid i\mid, P_0+P_1\,u\times i)}-1\right) \qquad (8)$$

where P_{supp} is the instantaneous electrical power supplied to the arc P_{supp} = ui, τ is the arc time constant, U_{arc} is the high-current arc-voltage constant, P_0 is the minimum cooling-power term, and P_1 scales the power-dependent cooling term. These definitions are used consistently in Table 2.

3.2.4. Proposed standard-based dielectric recovery algorithm

The dynamic arc equations determine the thermal behaviour of the breaker arc, but an additional dielectric-recovery decision is required to determine whether the breaker remains open or reignites after current interruption. The proposed algorithm supplies this decision by comparing the calculated breaker TRV with a standard-based dielectric-recovery screening reference. This reference is obtained from the circuit-breaker rated data and IEC four-parameter TRV envelope, because the manufacturer-specific dielectric recovery curve is not available for the investigated 500-kV SF6 circuit breaker.

The algorithm uses the following inputs: the instantaneous breaker current *i(t)*, contact voltage $u_{CB}(t)$, arc conductance *g(t)*, breaker opening command, conductance threshold g_{min}, IEC envelope parameters U_1, T_1, U_c, and T_2, reignition assessment window t_{window}, minimum reignition separation t_{gap}, and maximum permitted reignition count n_{max}. Its outputs are the breaker state, reignition occurrence, reignition count, and final TRV waveform.

The breaker is represented by three states. State 1 is the closed state, in which the breaker contact resistance is assigned a very small value. After the opening command, the breaker enters State 2, where the selected dynamic arc equation is solved and the contact resistance is updated from the instantaneous arc conductance. At each current zero, the algorithm checks whether the thermal condition $g < g_{min}$ is satisfied. If this condition is not satisfied, the breaker remains in State 2 and the arc continues.

If the thermal condition is satisfied, the breaker enters State 0 and the dielectric recovery check is activated. In State 0, the calculated contact voltage $|u_{CB}(t)|$ is continuously compared with the standard-based dielectric envelope $U_{env}(t)$. If $|u_{CB}(t)|$ remains below Uenv(t), the interruption is accepted as successful. If $|u_{CB}(t)|$ exceeds $U_{env}(t)$ within t_{window} and the time since the previous reignition is greater than t_{gap}, a reignition is declared. The breaker then returns to State 2, the arc conductance is reinitialized, and the arc equation is solved again until the next current zero. The reignition process is stopped when the interruption succeeds or when n_{max} is reached.

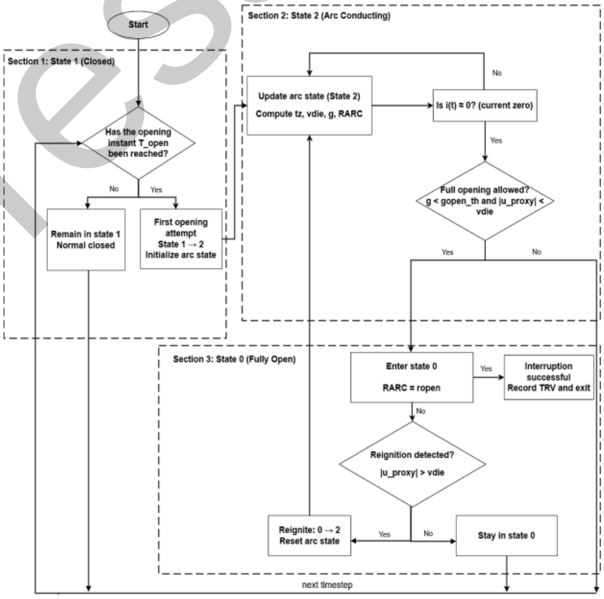

Fig. 6. Proposed standard-based dielectric recovery algorithm coupled with the dynamic arc models

3.2.5. Implemented arc-model and reignition parameters

Tables 2 and 3 summarize the parameter values for three arc models. The breaker is initialized in the closed state with a high conductance, transferred to the arc-conducting state at the prescribed opening instant, and allowed to return to the open state only when both the conductance threshold and dielectric-envelope conditions are satisfied. The Cassie-Mayr and Schwarz-Avdonin parameters are taken from the studies in [6, 17], whereas the Schavemaker parameters are not specifically fine-tuned and are used only for EMTP-ATP implementation and comparison.

In press

Table 2. Implemented model-specific arc parameters

Parameter	Cassie-Mayr	Schwarz-Avdonin	Schavemaker
P_0	8.8E3 W	4.0E6 W	3.0E5 W
τ_m	2.2E-7 s		
τ_c	8.0E-7 s		
U_{arc}	2350 V		2350 V
τ_0		1.5E-6 s	1.2E-5 s
a		0.17	
b		0.68	
P_1			0.8

Table 3. Common breaker-state, TRV-envelope, and reignition parameters

Parameter	Value used in all models
TRV envelope U_1	437846 V
TRV envelope T_1	2.189E-4 s
TRV envelope U_c	817313 V
TRV envelope T_2	8.756E-4 s
Minimum reignition separation t_{gap}	3.0E-5 s
Reignition assessment window t_{window}	2.0E-3 s
Maximum reignition count n_{max}	3
Open-state conductance threshold g_{min}	1.0E-3 S
Reinitialized reignition conductance g_{init}	0.08 S

The common values in Table 3 define the IEC four-parameter TRV screening envelope, the allowed reignition window, and the numerical thresholds used by the state machine. The selected U_1, T_1, U_c, and T_2 values correspond to the adopted 500-kV class TRV reference and are used only as a comparative dielectric-recovery criterion [13].

In practical terms, the implemented TRV envelope corresponds to a four-parameter reference with U_1 = 437.846 kV at T_1 = 218.923 µs and U_c = 817.313 kV at T_2 = 875.693 µs for the 500-kV circuit-breaker class as in IEC 62271-100. Reignition is allowed only within a 2-ms window after opening, with a minimum time separation of 30 µs between reignition attempts and a maximum of three reignitions. Full opening is accepted when the arc conductance falls below 1.0E-3 S and the contact voltage remains below the dielectric envelope.

4. TRV Simulation and Analysis

4.1. Ideal Switch

To represent a controlled switching condition, the breaker opening sequence is defined by phase-dependent timings of 17.8 ms for phase A, 24.4 ms for phase B, and 21.1 ms for phase C [2]. Under these conditions, the default ATP breaker model produces a maximum Phase-A TRV of 870 kV, which is used as the baseline case for subsequent comparison. For the selected opening instants, Phase A exhibits the most severe post-interruption voltage stress because its contact separation occurs under the least favorable combination of trapped reactor energy and recovery-voltage buildup. Phase A is therefore used as the primary comparison metric in the following discussion.

4.2. Dynamic Arc Circuit Breaker Model

The Schwarz-Avdonin model predicts a Phase-A peak TRV of 946 kV. Compared with the default ATP breaker case, this result indicates a noticeably higher switching severity when breaker arc dynamics and dielectric recovery are represented explicitly.

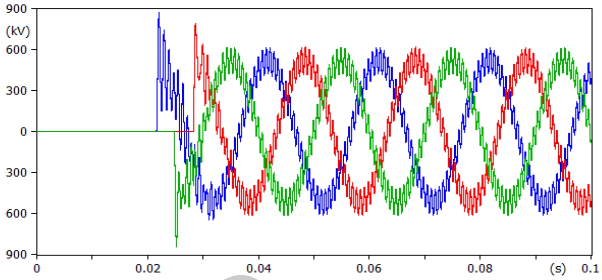

Fig. 7. TRV across the reactor circuit breaker using the default ATP breaker model

The Schavemaker model yields the most severe simulation result among the investigated arc models, with the Phase-A peak TRV reaching 1600 kV. This high value is mainly associated with the adopted Schavemaker cooling-power expression and time constant, which keep the post-current-zero conductance and reignition susceptibility higher than in the other two models. Consequently, the Schavemaker result should be interpreted as a sensitivity boundary for the selected parameter set rather than as a validated breaker-specific prediction. After implementing the three breaker representations, the resulting peak Phase-A TRV values are summarized in Table 4.

Table 4. Comparison of phase-A peak TRV for different breaker representations

Model	ATP default	Cassie-Mayr	Schwarz-Avdonin	Schavemaker
Peak TRV (kV)	870	874	946	1600

The ATP default breaker represents switching as an ideal open-close operation, while the Cassie-Mayr, Schwarz-Avdonin, and Schavemaker models describe arc conductance as a time-varying quantity linked to the instantaneous arc state. These dynamic models therefore include arc quenching, dielectric recovery, and reignition effects neglected by the ideal ATP breaker. As a result, the Phase-A peak TRV increases from 870 kV with the ATP breaker to 874 kV, 946 kV, and 1600 kV with the Cassie-Mayr, Schwarz-Avdonin, and Schavemaker models, respectively. The wide spread among the dynamic models confirms that arc-parameter selection is a controlling factor in black-box breaker studies. In [6], the TRV ranged from 1.8 pu to 2.5 pu across the investigated cases. In addition, the TRV level specified in standard [13] falls between 817 kV and

in press

1031 kV, which indicates that the Cassie-Mayr result is within an acceptable range.

For the mitigation study, Cassie-Mayr is used as the practical reference model because it covers both high-current and near-current-zero regions and gives a stable comparative base close to the ATP baseline while still including explicit arc dynamics. This choice is not a validation of Cassie-Mayr over the other models, but an application-oriented basis for comparing mitigation options without claiming manufacturer-specific calibration.

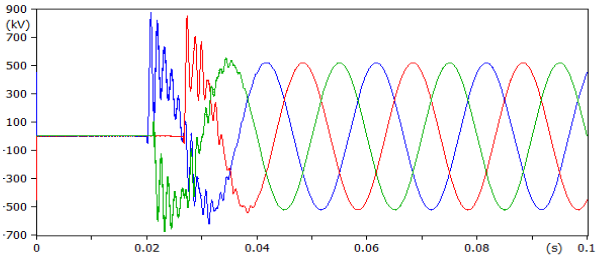

Fig. 8. Three-phase voltage oscillations obtained with the Cassie-Mayr model

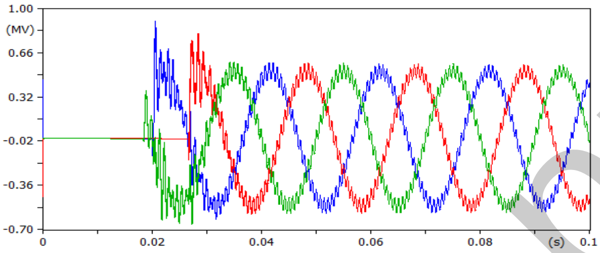

Fig. 9. Three-phase voltage oscillations obtained with the Schwarz-Avdonin model

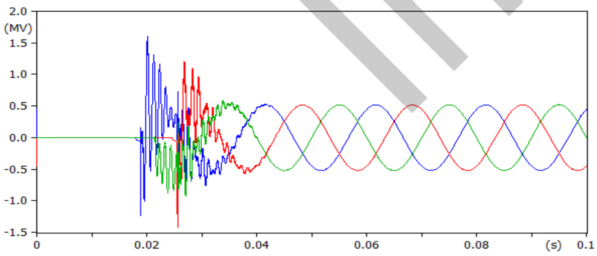

Fig. 10. Three-phase voltage oscillations obtained with the Schavemaker model

4.3. Practical Mitigation Measures

Several mitigation methods are discussed in IEEE Std C37.015 and related shunt-reactor switching studies, including controlled switching, surge arresters, neutral-side switching arrangements, and insulation-coordination measures [1, 2]. The present paper does not optimize all possible combinations; instead, it compares two readily implementable network-side options in the same ATPDraw framework: a surge arrester and a combined surge-arrester/neutral-grounding-disconnector configuration.

4.3.1. Surge arrester installation

The first mitigation measure considered in this study is the installation of a metal-oxide surge arrester at the reactor-side breaker terminal. In ATP, the arrester is represented as a nonlinear voltage-dependent element that carries negligible current during normal operation but conducts strongly when the post-interruption voltage approaches the residual-voltage region (Fig. 11).

Using the Cassie-Mayr model as the detailed breaker representation, the surge arrester reduces the Phase-A peak TRV from 874 kV to 846 kV. This corresponds to a reduction of approximately 3.2 percent, indicating that only the arrester is not an effective solution in clamping the post-interruption overvoltage in the selected study case. Fig. 13 indicates that the surge arrester limits the highest post-interruption voltage excursion and visibly clips the most severe portion of the waveform. The remaining oscillation confirms that the arrester mitigates, but does not eliminate, the transient behavior associated with the switching event.

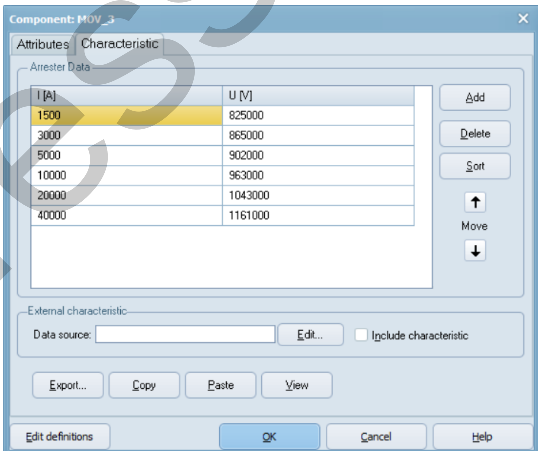

Fig. 11. Surge arrester characteristic V-I

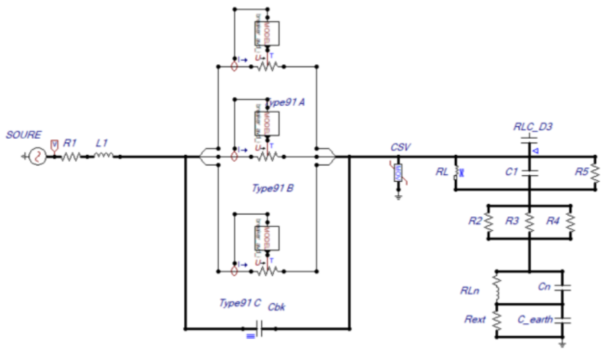

Fig. 12. Simulation model including the surge arrester mitigation option

4.3.2. Installation of shunt-reactor neutral-grounding disconnector

The second mitigation option is the installation of a neutral-grounding disconnector in order to modify the neutral-side operating condition of the shunt reactor. In

In press

this study, the disconnector is evaluated together with the surge arrester so that the incremental benefit of the combined configuration can be compared with the arrester-only case.

After implementing the neutral-grounding disconnector together with the surge arrester, the Phase-A peak TRV is further reduced to 774 kV. Relative to the 874-kV Cassie-Mayr base case, this corresponds to a reduction of approximately 11.4%. Relative to the arrester-only case, the additional reduction is approximately 8.2%.

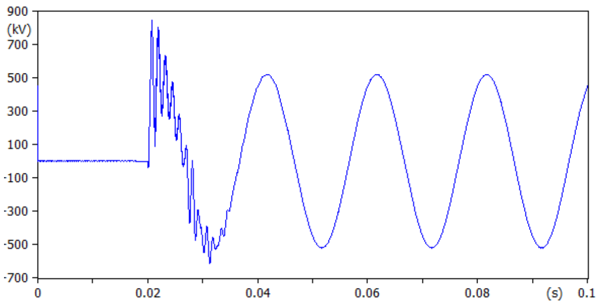

Fig. 13. Phase-A TRV after surge arrester installation

Physically, the combined configuration modifies both the overvoltage clamping behaviour and the neutral-side transient response of the reactor, thereby lowering the voltage appearing across the breaker contacts.

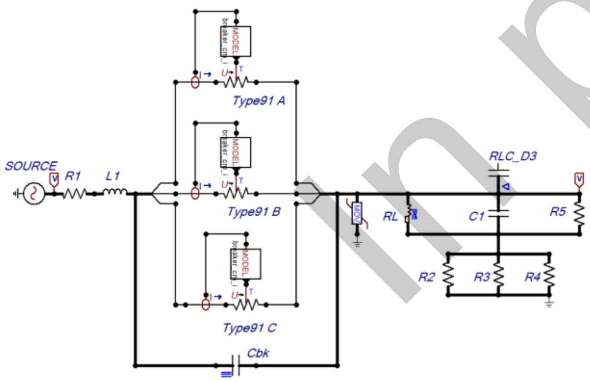

Fig. 14. Simulation model including both surge arrester and shunt-reactor neutral grounding disconnector

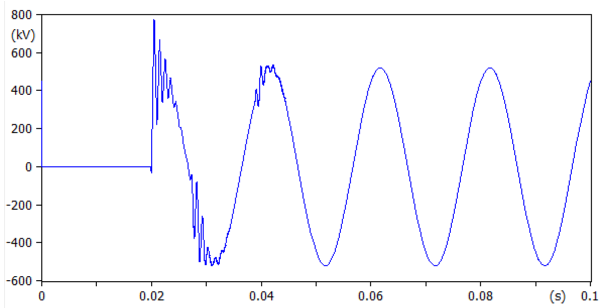

Fig. 15. Phase-A TRV after applying both the surge arrester and neutral-grounding disconnector

4.4. Benchmarking, Parameter Sensitivity, and Limitations

The reliability of the simulation framework was checked through benchmarking rather than through manufacturer test records, which were not available for the studied breaker. The first check is theoretical: the implemented Cassie-Mayr, Schwarz-Avdonin, and Schavemaker equations and the reignition logic follow published black-box modelling procedures [5, 7, and 8]. The second check is standards-based: the calculated recovery voltage is evaluated against the IEC four-parameter TRV envelope and interpreted using the shunt-reactor switching guidance of IEEE Std C37.015 [1, 13]. The third check is behavioral: the dynamic arc models predict equal or higher TRV duty than the ideal ATP switch, and the surge arrester and neutral-grounding configuration reduce the peak TRV in the expected direction, which is consistent with published shunt-reactor switching studies [2-4].

The most influential parameters are the source Thevenin impedance, the reactor-side parasitic capacitances, the arc time constants, and the cooling-power terms. Increasing the effective source inductance or reducing the damping resistance generally increases the RRRV. Increasing the arc time constant, reducing P_0, or selecting cooling-power coefficients that slow conductance decay increases the probability of reignition and raises the peak TRV. This explains why the Schavemaker case gives a much higher value than the Cassie-Mayr and Schwarz-Avdonin cases under the adopted parameters. Therefore, the absolute peak values should not be used directly as breaker ratings unless the black-box parameters are calibrated against type-test or field oscillogram data.

The main limitation of the study is that breaker-specific dielectric recovery and measured field waveforms were not available. Future work should include parameter sweeps over the arc-model constants, measured station capacitances, controlled-switching scatter. Such validation would allow the present comparative ATPDraw framework to be converted into a calibrated breaker-duty assessment for a specific installation.

5. Conclusions

This paper has presented an application-oriented ATPDraw framework for assessing 500-kV shunt-reactor switching with different levels of breaker-model detail. The comparison among the built-in ATP breaker, the Cassie-Mayr model, the Schwarz-Avdonin model, and the Schavemaker model shows that explicit arc modelling can predict higher TRV than the idealized breaker representation and can capture arc-dynamic effects that are neglected by the default switch model. For the investigated case, the Phase-A peak TRV is 870 kV with the ATP breaker, 874 kV with Cassie-Mayr, 946 kV with Schwarz-Avdonin, and 1600 kV with Schavemaker. The Schavemaker result highlights the sensitivity of black-box studies to the selected cooling-power and time-constant parameters.

In press

The mitigation study further demonstrates that the selected surge arrester reduces the Phase-A peak TRV to 840 kV, while the combined arrester and neutral-grounding disconnector reduces it to 774 kV. These results support the practical conclusion that both breaker-model fidelity and network-side mitigation strongly influence the assessed switching severity in transmission-substation studies. Because the arc parameters were not calibrated against manufacturer test records or field oscillograms, the numerical values should be used for comparative engineering assessment, while future work should focus on measured validation and systematic parameter sensitivity.

References

[1] IEEE Guide for the Application of Shunt Reactor Switching, IEEE Std C37.015-2017 (Revision of IEEE Std C37.015-2009), pp. 1-63, Mar. 2018. https://doi.org/10.1109/IEEESTD.2018.8320990

[2] P. T. Tran and D. N. Vo, Effects of transient recovery voltage and degradation solutions when opening shunt reactor at 500 kV O Mon substation, VNUHCM Journal of Engineering and Technology, vol. 2, no. 2, pp. 86-96, Oct. 2019. https://doi.org/10.15419/stdjet.v2i2.500

[3] L. Prikler, G. Bán, and G. Bánfai, EMTP models for simulation of shunt reactor switching transients, International Journal of Electrical Power & Energy Systems, vol. 19, pp. 235-240, May 1997. https://doi.org/10.1016/S0142-0615(96)00050-6

[4] Z. Ma, C. A. Bliss, A. R. Penfold, A. F. W. Harris, and S. B. Tennakoon, An investigation of transient overvoltage generation when switching high-voltage shunt reactors by SF6 circuit breaker, IEEE Transactions on Power Delivery, vol. 13, no. 2, pp. 472-479, Apr. 1998. https://doi.org/10.1109/61.660917

[5] S. M. Ghafourian, Switching transients in large offshore wind farms: System components modeling, Ph.D. dissertation, School of Electrical and Electronic Engineering, The University of Manchester, Manchester, U.K., 2013.

[6] EVN PECC4, Study on Solutions to Ensure Safe Operation of Circuit Breakers for Shunt Reactors in the Transmission Grid, Volume 1: Project Report, 2024.

[7] S. Y. Leung, L. A. Snider; and C. S. M. Wong, SF6 generator circuit breaker modeling, in Proceedings International Conference on Power Systems Transients (IPST'05), Montreal, Canada, Jun. 2005.

[8] R. Elbahy, A. Abdelbaset, M. Hammoda, M. H. Abdel-Rahman, and E. A. Badran, Black-box modeling of HVCB using ATPDraw, in Proceedings 24th International Middle East Power System Conference (MEPCON), Mansoura, Egypt, pp. 1-5, Dec. 2023. https://doi.org/10.1109/MEPCON58725.2023.10462461

[9] M. Popov and L. van der Sluis, Comparison of two vacuum circuit breaker arc models for small inductive current switching, in Proceedings International Symposium on Discharges and Electrical Insulation in Vacuum (ISDEIV), vol 2, pp. 438-441, Sep. 2000. https://doi.org/10.1109/DEIV.2000.879033

[10] A. Greenwood and M. Glinkowski, Voltage escalation in vacuum switching operations, IEEE Transactions on Power Delivery, vol. 3, no. 4, pp. 1698-1706, Oct. 1988. https://doi.org/10.1109/61.193974

[11] M. T. Glinkowski, M. R. Gutierrez, and D. Braun, Voltage escalation and reignition behavior of vacuum generator circuit breakers during load shedding, IEEE Transactions on Power Delivery, vol. 12, iss. 1, pp. 219-226, Jan. 1997. https://doi.org/10.1109/61.568244

[12] S.-C. Kam, Modelling of restriking and reignition phenomena in three-phase capacitor and shunt reactor switching, M.S. thesis, Queensland University of Technology, Brisbane, QLD, Australia, 2006.

[13] IEC 62271-100:2021, High-Voltage Switchgear and Controlgear - Part 100: Alternating-current circuit-breakers, Jul. 2021.

[14] R. D. Garzon, High Voltage Circuit Breakers: Design and Applications. New York, NY, USA: Marcel Dekker, 1996.

[15] E. Haginomori, T. Koshiduka, J. Arai, and H. Ikeda, Power System Transient Analysis: Theory and Practice Using Simulation Programs (ATP-EMTP). Hoboken, NJ, USA: Wiley, 2016.

[16] J. A. Martinez-Velasco, Power System Transients: Parameter Determination. Boca Raton, FL, USA: CRC Press, 2009.

[17] I. Uglešić, B. Filipović-Grčić, V. Milardić, and I. Ivanković, Transient recovery voltage of 400 kV SF_6 circuit breaker when clearing shortline fault, in Proceedings 16th International Symposium on High Voltage Engineering, 2009.

[18] PEEC2, Large Grid Modeling - Vietnam 500-220kV Power System, 2015. [Online]. Available: https://www.emtp.com/exchange-platform/Large-Grid-Modeling---Vietnam-500-220kV-Power-System-209

In press